IMPEDANCE ANALYSIS OF A TIGHT EPITHELIUM USING A DISTRIBUTED RESISTANCE MODEL

CHRIS CLAUSEN, SIMON A. LEWIS, AND JARED M. DIAMOND, *Department of Physiology, School of Medicine, University of California, Los Angeles, California 90024 U.S.A.*

ABSTRACT This paper develops techniques for equivalent circuit analysis of tight epithelia by alternating-current impedance measurements, and tests these techniques on rabbit urinary bladder. Our approach consists of measuring transepithelial impedance, also measuring the DC voltage-divider ratio with a microelectrode, and extracting values of circuit parameters by computer fit of the data to an equivalent circuit model. We show that the commonly used equivalent circuit models of epithelia give significant misfits to the impedance data, because these models (so-called "lumped models") improperly represent the distributed resistors associated with long and narrow spaces such as lateral intercellular spaces (LIS). We develop a new "distributed model" of an epithelium to take account of these structures and thereby obtain much better fits to the data. The extracted parameters include the resistance and capacitance of the apical and basolateral cell membranes, the series resistance, and the ratio of the cross-sectional area to the length of the LIS. The capacitance values yield estimates of real area of the apical and basolateral membranes. Thus, impedance analysis can yield morphological information (configuration of the LIS, and real membrane areas) about a living tissue, independently of electron microscopy. The effects of transport-modifying agents such as amiloride and nystatin can be related to their effects on particular circuit elements by extracting parameter values from impedance runs before and during application of the agent. Calculated parameter values have been validated by independent electrophysiological and morphological measurements.

INTRODUCTION

In this paper we develop methods for alternating current (AC) equivalent circuit analysis of tight epithelia. These methods are capable of resolving separate membrane conductances, measuring true areas of folded membranes, and nondestructively monitoring changes in membrane geometry.

We turned to AC analysis because of the technical problems in achieving the three above-mentioned goals by direct current (DC) methods. From DC measurements of transepithelial conductance alone, it is not generally possible to separate this conductance into the conductances of the apical and basolateral membranes and junctions. In very tight epithelia, for which junctional conductance is negligible, this resolution can be achieved by supplementing transepithelial conductance measurements with a single microelectrode measurement to obtain the so-called voltage-divider ratio (ratio of basolateral to apical membrane conductance). In leaky epithelia a two-microelectrode method, cable analysis, may be able to resolve

Dr. Lewis' present address is Department of Physiology, Yale Medical School, 333 Cedar Street, New Haven, Conn. 06510

the membrane conductances, but this method often yields only crudely approximate answers, due to problems in accurately determining electrode position, to geometrical complexities such as tissue folding, and to simplifications in modeling lateral current flow (cf. Eisenberg and Johnson, 1970, Frömter, 1972; Peskoff, 1979).

A general failure of these DC methods is that they do not measure real membrane area, and hence cannot yield values of membrane conductance per unit area or distinguish changes in area from changes in membrane permeability properties. These are ubiquitous problems in epithelial studies, as epithelia contain both macroscopic and microscopic folds, such that the true cell membrane area exceeds the nominal chamber area by an unknown factor that can vary with physiological conditions (cf. Forte, et al., 1975). Nor do DC methods give information about membrane geometry, such as lateral intercellular space width, an important parameter in epithelial water transport.

Use of AC methods to measure transepithelial impedance and interpret it in terms of a morphologically based equivalent circuit model offers three potential advantages. First, under favorable conditions, this technique can resolve separate membrane conductances without additional measurements. Second, it also resolves separate membrane capacitances. Since the capacitance per unit of area of diverse biological membranes is relatively constant around 1 $\mu F/cm^2$ (range for nonfolded biological membranes, 0.8–1.2 $\mu F/cm^2$: Davson, 1964; and Cole, 1972), measured capacitances yield values for real membrane areas. Finally, some morphological structures such as lateral spaces can be modeled as so-called distributed circuit elements, whose impedance is a function of the structures' geometry, thereby permitting one continuously to monitor morphology in living cells.

AC impedance analysis has been profitably applied to numerous cells, including erythrocyte, marine eggs, nerve (for review, see Cole, 1972), and notably skeletal muscle (Falk and Fatt, 1964; Valdiosera et al. 1974*b*). However, the few AC studies of epithelia encountered several formidable difficulties. First, most of these pioneering applications to epithelia measured impedance by using step inputs of applied current and analyzing the voltage response in the time domain, or by use of Fourier analysis, converting the time response into the frequency response (Teorell and Wersall, 1945; Teorell, 1946; Rehm et al., 1976; Noyes and Rehm, 1970; Smith, 1975). This step-response method has disadvantages compared to that of measuring the impedance by using sinusoids (or Gaussian or pseudo-random binary noise), for reasons to be discussed below (pp. 299–300). Second, it is a difficult problem to formulate for epithelia an equivalent circuit model of sufficient realism so that its circuit parameters could correspond to real biological membrane properties. For example, frog skin, a multi-cell-layered epithelium with complex morphology, has been modeled in impedance studies as a parallel resistor-capacitor (RC) combination and series resistor, with deviations from ideal circuit behavior handled by postulating nonideal capacitance (Brown and Kastella, 1965; Smith, 1975). In these circuits, the parameters do not correspond to individual membrane properties. Finally, the commonly used "impedance locus" or "Nyquist" representation of data has disadvantages for epithelia, to be discussed below (p. 302).

Before impedance analysis can be used and trusted to answer unsolved questions for epithelia, numerous methodological problems must first be solved, and the new methods must be validated by showing that they yield results confirmed by independent techniques. The solving of the problems and validation of the methods constitute the subjects of the present

paper. The tight epithelium we chose to study, rabbit urinary bladder, will not illustrate the full advantages of impedance analysis, as transepithelial AC measurements must be supplemented in this epithelium by microelectrode measurement of the voltage-divider ratio, α, to extract circuit parameters. Thus, in this tissue, AC techniques offer no advantage for resolving membrane conductances unrelated to membrane area. However, the AC techniques do yield other quantities that DC techniques do not (real membrane areas and hence conductances per unit area, LIS width, and series resistance). We mention explicitly at the outset that our techniques suffice in principle only for tight epithelia: impedance analysis of leaky epithelia will require additional measurements.

Our presentation is organized as follows. First, we derive a new "distributed model" for an epithelium's equivalent electrical circuit, because effects associated with distributed resistors prove to be conspicuous in epithelial impedance measurements. Next, we describe experimental methods, then methods of data analysis. Finally, we present experimental results, and conclude with a discussion.

DERIVATION OF THE DISTRIBUTED MODEL

To describe current flow in a biological tissue by linear circuit analysis, one must first model the preparation by an equivalent electrical circuit made up of capacitors and resistors, corresponding to membrane capacitances and conductances. This modeling poses two major problems: realism and undetermined parameters.

Realism

Only if the model circuit elements correspond to morphological structures of the tissue can fitted model parameters (capacitor and resistor values) be good estimates of actual membrane parameters. (The problems in developing a realistic model are well illustrated by the history of equivalent circuit analysis in frog skeletal muscle: Valdiosera et al., 1974*a*; and Mathias et al., 1977).

Undetermined Parameters

If the black-box behavior of an electrical circuit can be described by equations containing fewer parameters than there are circuit elements, the circuit model is said to contain undetermined parameters. For example, an equivalent circuit of an epithelium (e.g., Fig. 1 *B*) must consider at least two current pathways: a paracellular path (via the junctions and lateral spaces, or else via an edge-damage shunt) and a transcellular path (via apical cell membrane, cells, and basolateral cell membrane). It is impossible to separate these two paths by transepithelial techniques alone. The two parallel resistive paths lump together mathematically: for example, the six-element circuit of Fig. 1 *B* is completely described by an equation with only five parameters (see below, p. 314). Thus, by themselves, the transepithelial techniques disucssed in this paper are adequate only for tight epithelia with negligible junctional conductance and negligible edge damage. Impedance analysis of leaky epithelia, or ones with edge damage, will require additional intracellular measurements or else direct knowledge of junctional and shunt conductances.

Fig. 1 *B* (after Lewis and Diamond, 1976) is a recent epithelial circuit model. It represents an epithelium as two parallel RC circuits in series (to represent the apical and basolateral

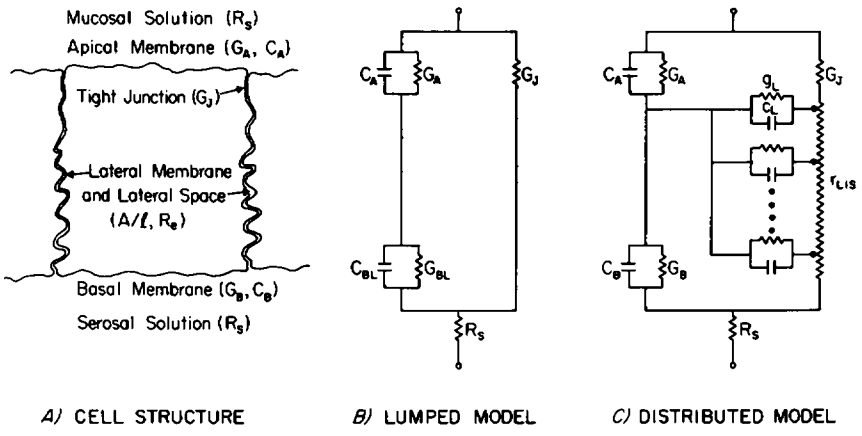

FIGURE 1 (*A*) Schematic representation of rabbit urinary bladder, showing the one functional cell layer. Note the narrow, tortuous, lateral intracellular space. The symbols in parentheses indicate the distributed model circuit parameters that describe the electrical properties of each membrane structure (see Theory section). (*B*) The "lumped" model equivalent circuit. The apical membrane is modeled as a lumped RC combination. The basal plus lateral membranes are also treated as a lumped circuit; the resistance down the lateral spaces is assumed negligible and ignored. (*C*) The "distributed" model equivalent circuit. It differs from the lumped model in that the narrow dimensions of the lateral space are taken into consideration by treating the lateral membrane as a distributed impedance. See Table I for description of the symbols.

membranes), with a parallel resistor (to represent junctional and shunt conductance) and series resistor (to represent unstirred layers and connective tissue). This model, which we shall refer to as the "lumped model," has the following impedance (see Table I for definition of parameters):

$$Z_T = R_S + \left[G_J + \frac{Y_A Y_{BL}}{Y_A + Y_{BL}}\right]^{-1}. \quad (1)$$

However, a morphologically significant feature which this lumped model still neglects is the LIS, which are bordered by the lateral portion of the basolateral membrane. In rabbit gallbladder the LIS are sometimes sufficiently narrow so that the resistivity of the solution in them contributes significantly to transepithelial resistance (Smulders et al., 1972). In mammalian urinary bladder, the LIS are only ~100 Å wide but 20 μm long (Richter and Moize 1963; Walker 1960; Porter and Bonneville, 1973), so that the expected resistance to current flow along the length of the LIS is ~130 Ω-cm^2, assuming a solution resistivity of ~64 Ω-cm (see footnote 1). Yet the membrane impedance of rabbit urinary bladder decreases at high frequencies (≥200 Hz) to ≤130 Ω-cm^2 due to the lateral membrane capacitance. At low frequencies (≤10 Hz), lateral membrane current is determined largely by lateral membrane resistance, which is much higher than the resistance of the LIS. Thus, the

[1] We can obtain a rough estimate of A/ℓ by assuming cuboidal cellular geometry: $A/\ell \simeq$ [(number of cells) · 4 · (cell width) · (½)(LIS width)]/(LIS length). If we assume that cells are roughly 20 μm on each side, and that LIS width is 100 Å, then for 1 cm^2 of preparation: $A/\ell \simeq \{[1/(20 \times 10^{-4})]^2 \cdot 4 \cdot (20 \times 10^{-4}) \cdot (\frac{1}{2})(100 \times 10^{-8})\}/(20 \times 10^{-4}) = 0.5$ cm.

The serosal solution resistivity R_e was measured as 64 Ω-cm at 37°C. Hence the LIS resistance to current flow is: $R_{LIS} = R_e/(A/\ell) = 64/0.5 \sim 130\,\Omega$.

TABLE I

SYMBOLS

		Units
	Circuit Parameters	
Z_T	Transepithelial impedance.	Ohms
G_T	Transepithelial conductance. $G_T = R_T^{-1}$	$Ohms^{-1}$
Y_A	Apical membrane admittance. $Y_A = G_A + sC_A = Z_A^{-1}$	
	G_A Apical membrane conductance.	$Ohms^{-1}$
	C_A Apical membrane capacitance.	Farads
Y_B	Basal membrane admittance. $Y_B = G_B + sC_B = Z_B^{-1}$	
	G_B Basal membrane conductance.	$Ohms^{-1}$
	C_B Basal membrane capacitance.	Farads
Y_{BL}	Basolateral membrane admittance. $Y_{BL} = G_{BL} + sC_{BL} = Z_{BL}^{-1}$	
	G_{BL} Basolateral membrane conductance.	$Ohms^{-1}$
	C_{BL} Basolateral membrane capacitance.	Farads
	In distributed model: $Y_{BL} = Y_B(1 + S_L/S_B)$	
G_J	Junctional (paracellular) conductance.	$Ohms^{-1}$
R_S	Series resistance in unstirred layers.	Ohms
s	Laplace transform variable. In sinusoidal steady state: $s = j\omega$, $j = \sqrt{-1}$, and $\omega = 2\pi \cdot$ frequency.	$Rad\text{-}s^{-1}$
	Lateral Space (LIS) Parameters	
S_L/S_B	Lateral to basal membrane area ratio.	—
A/ℓ	LIS cross-sectional area to length ratio.	cm
R_e	Resistivity of solution filling LIS.	Ohm-cm
	Symbols Used in the Derivation of the Distributed Model	
x	Distance along LIS measured from junction.	cm
ℓ	Length of LIS.	cm
V_0	Transepithelial potential due to applied current.	Volts
V_i	Intracellular potential due to applied current.	Volts
$V_e(x)$	LIS potential due to applied current.	Volts
I_T	Applied transepithelial current.	Amps
$i_i(x)$	Current that flows intracellularly.	Amps
$i_e(x)$	Current that flows in LIS.	Amps
$i_L(x)$	Current that crosses the lateral membrane.	Amps
r_{LIS}	Resistance per unit length of LIS.	$Ohm\text{-}cm^{-1}$
y_L	Lateral membrane admittance per unit length of LIS. $y_L = g_L + sc_L$,	
	g_L Lateral membrane conductance per unit length of LIS.	$Ohm^{-1}\text{-}cm^{-1}$
	c_L Lateral membrane capacitance per unit length of LIS.	$Farads\text{-}cm^{-1}$
Γ	Reciprocal length constant of lateral membrane. $\Gamma = \sqrt{r_{LIS}\, y_L}$.	cm^{-1}
S	$S^2 = (S_L/S_B) \cdot (\ell/A) \cdot R_e Y_B$.	—
T	$T^2 = (S_L/S_B) \cdot (A/\ell) \cdot (Y_B/R_e)$.	$Ohms^{-1}$

This table defines the symbols used when describing the lumped and distributed models. The units are all for 1 cm^2 of preparation.

narrowness of the LIS constitutes a "distributed" resistance in series with the lateral but not basal portion of the basolateral cell membrane, restricts current flow at high but not low frequencies, and causes the lumped model seriously to underestimate basolateral capacitance. In the high-frequency extreme, where membrane impedance is negligible compared to LIS resistance, most current flow across the basolateral membrane would be confined to the basal portion.

Effects of this type can be termed "distributed" effects. They are expected to occur

whenever the resistance to current flow down a narrow, fluid-filled space bounded by a membrane becomes comparable to that membrane's impedance. Generally, cells can be considered to have negligible intracellular resistance due to the relatively large cell volume and low intracellular resistivity, hence intracellular distributed effects can perhaps be ignored. However, when the dimensions of the spaces become small, the relative space resistance becomes comparable to that of the membrane, and the distributed resistance must be considered. As we shall show, distributed effects show up clearly in impedance measurements from rabbit urinary bladder.

For these reasons we developed a new "distributed" model of an epithelium, illustrated in Fig. 1 *C*. The apical and basal membranes are still treated as lumped impedances; however, the lateral membrane is treated as a distributed impedance (distributed along the LIS), and the LIS, as a distributed resistor. The cell interior is treated as equipotential due to the large cell dimensions (i.e., for all frequencies of interest, the intracellular resistance is assumed to be a negligible barrier to current flow compared with the cell membranes or LIS: see footnote 2).

We now derive the differential equation describing current flow in this distributed model, which resembles the familiar distributed model for current flow in nerve (Cole, 1972). Table I explains symbols used in the derivation.

The potential gradient along the LIS is:

$$\frac{dV_e}{dx} = -r_{LIS} i_e. \tag{2}$$

This expression represents solely the potential due to current flow along the resistive path that the fluid in the LIS constitutes. LIS resistance is calculated from LIS cross-sectional area and length, assuming LIS width to be constant over the length. This assumption seems reasonable for rabbit urinary bladder, as electron micrographs show LIS width to be virtually constant at around 100 Å over the whole length.

Since the cell interior is assumed equipotential,[2] the intracellular potential must satisfy:

$$\frac{dV_i}{dx} = 0. \tag{3}$$

By conservation of current, all current that enters the LIS across the lateral membrane must come from the cell interior:

$$\frac{di_e}{dx} = -\frac{di_i}{dx} = i_L. \tag{4}$$

The lateral transmembrane potential is given by:

$$V_i - V_e = i_L / y_L. \tag{5}$$

---

[2]That is, we assume that the major barrier to current flow is the impedance of the membranes, and we neglect resistive voltage drops due to the finite resistivity of the cell interior. How valid is this assumption? The worst error due to this assumption will occur at high frequencies of applied current, since intracellular resistance is virtually independent of frequency, but membrane impedance decreases with frequency due to capacitance current. If one uses typical cell dimensions, and assumes intracellular resistivity of roughly 1,000 Ω-cm—an order of magnitude greater than the extracellular resistivity—then one calculates that only 10% of the transepithelial voltage drop would be intracellular even at the highest current frequency used (10,000 Hz).

The boundary condition for the potential in the LIS at their open end—i.e., at the level of the basal membrane—is:

$$V_e(\ell) = I_T R_S. \tag{6}$$

Note that this potential differs from zero because of the series impedance, considered purely resistive, of the unstirred layers and basal cell layers. Lewis et al. (1976*a*, *b*) showed that the resistance of these basal cell layers is less than 1% of that of the transporting cell layer. Some of the series resistance must be associated with the unstirred layer adjacent to the apical membrane, but in Fig. 1 *C* we arbitrarily place the entire series resistance on the basal side, as its location cannot be determined from transepithelial measurements alone.

For generality, the paracellular current (negligible in rabbit urinary bladder) that bypasses the cells and enters the LIS via the junctions is written as:

$$i_e(0) = G_J[V_o - V_e(0)]. \tag{7}$$

The apical and basal transmembrane potentials are determined by the currents crossing them and their respective admittances:

$$\begin{aligned} V_i - V_o &= -i_i(0)/Y_A \\ V_i - V_e(\ell) &= i_i(\ell)/Y_B. \end{aligned} \tag{8}$$

Finally, conservation of current equates the total transepithelial current at the apical boundary (current across apical membrane, plus paracellular current across junction) and at the basal boundary (current across basal membrane, plus current out the open basal end of the LIS):

$$I_T = i_i(0) + i_e(0) = i_i(\ell) + i_e(\ell). \tag{9}$$

Subtracting Eq. 2 from Eq. 3, differentiating with respect to x, and substituting Eqs. 4 and 5 yield:

$$\frac{d^2}{dx^2}(V_i - V_e) = \Gamma^2(V_i - V_e). \tag{10}$$

Eqs. 3 and 10 plus the boundary conditions let one solve for the extra- and intracellular potentials $V_e(x)$ and V_i in terms of total transepithelial current, I_T, and transepithelial voltage V_o. The ratio of V_o to I_T is the impedance:

$$Z_T = R_S + \left[Y_A + G_J \frac{Y_B + Y_A \operatorname{sech} \Gamma\ell + \frac{\Gamma}{r_{LIS}} \tanh \Gamma\ell}{Y_B + \left[\frac{\Gamma}{r_{LIS}} + \frac{r_{LIS}}{\Gamma} Y_B G_J\right] \tanh \Gamma\ell + G_J(1 - \operatorname{sech} \Gamma\ell)} \right]^{-1} + \frac{1 + G_J\left[\frac{r_{LIS}}{\Gamma} \tanh \Gamma\ell + (1 - \operatorname{sech} \Gamma\ell)/Y_A\right]}{Y_B + G_J(1 + Y_B/Y_A) + \left[\frac{r_{LIS}}{\Gamma} Y_B G_J + \frac{\Gamma}{r_{LIS}}(1 + G_J/Y_A)\right] \tanh \Gamma\ell} \tag{11}$$

Eq. 11 can be simplified by assuming the basal and lateral membranes share the same membrane properties (conductance and capacitance) per unit area, and thereby expressing lateral membrane admittance in terms of basal membrane admittance. However, this requires introducing two morphological (not electrical) parameters, and hence offers the possibility of extracting values of these *morphological* parameters by fitting measured impedances to the model equation. The two parameters are: S_L/S_B, ratio of lateral membrane area to basal membrane area; and A/ℓ, ratio of cross-sectional area of length of the LIS. With these substitutions, and assuming the LIS to be filled with serosal bathing solution of resistivity R_e, Eq. 11 becomes:

$$Z_T = R_S + \left[Y_A + G_J \frac{Y_B + Y_A \operatorname{sech} S + T \tanh S}{Y_B + (1 + Y_B G_J/T) \tanh S + G_J(1 - \operatorname{sech} S)}\right]^{-1} + \frac{1 + G_J[(\tanh S)/T + (1 - \operatorname{sech} S)/Y_A]}{Y_B + G_J(1 + Y_B/Y_A) + [Y_B G_J/T + T(1 + G_J/Y_A)] \tanh S} \quad (12)$$

where S and T are defined as: $S^2 = (S_L/S_B)(\ell/A)(R_e Y_B)$, $T^2 = (S_L/S_B)(A/\ell)(Y_B/R_E)$.

In practice, we made a further simplification to reduce by one the number of model parameters: we assumed that the epithelial cells are can-shaped (i.e., closed right circular cylinders), so that $C_B \sim C_A$, and C_{BL} may be calculated as $C_A(1 + S_L/S_B)$. It turns out that this simplification does not reduce the goodness of fit of the distributed model to impedance measurements in rabbit urinary bladder.

Now consider two limiting cases of Eq. 12. First, when junctional conductance G_J is negligible (as is true in rabbit urinary bladder), Eq. 12 greatly simplifies to:

$$Z_T = R_S + Y_A^{-1} + (Y_B + T \tanh S)^{-1}. \quad (13)$$

The second limiting case is when LIS resistance per unit length becomes negligible—e.g., when the LIS dilate and A/ℓ becomes large. In this limit Eq. 13 simplifies to:

$$Z_T = R_S + Y_A^{-1} + [Y_B(1 + S_L/S_B)]^{-1}. \quad (14)$$

This expression is identical to the impedance derived from the lumped model (Eq. 1) in the limit where $G_J \to 0$, as the lumped basolateral admittance can be represented as:

$$Y_{BL} = Y_B(1 + S_L/S_B). \quad (15)$$

Thus, the distributed model simplifies to the lumped model when the LIS are wide.

Under what biological conditions is the distributed effect likely to be significant? Fig. 2 shows four theoretical impedance curves, calculated by inserting into Eq. 13 or 14 typical circuit parameters determined for rabbit urinary bladder by Lewis et al. (1976*b*), and using four different values for A/ℓ. Fig. 2 yields three conclusions: First, the distributed effect, expressed as the deviation in the impedance plot from the result of the lumped model, appears only at middle to high frequencies. Second, the deviations are much greater in the phase Bode plot (Fig. 2 above) than magnitude Bode plot (Fig. 2 below; see p. 302 for explanation of these Bode plots). Third, given the circuit parameter values of rabbit urinary bladder, A/ℓ must be ≤ 1 cm (for 1 cm^2 of tissue) for the distributed effect to be detectable by impedance

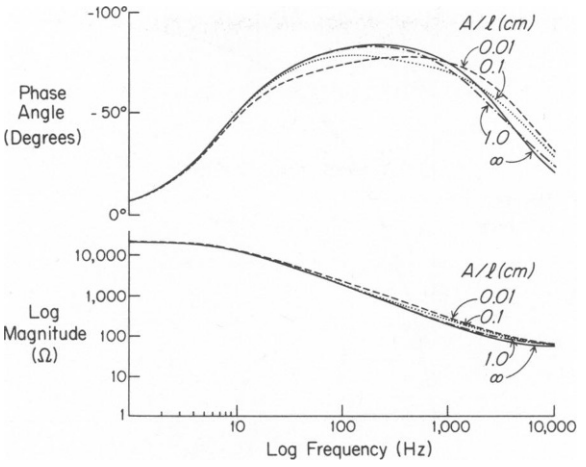

FIGURE 2 Effect of varying the distributed parameter A/ℓ on the impedance predicted by the distributed model. The top part of the figure shows the phase and the bottom shows the log magnitude, both as a function of frequency. Values of A/ℓ are shown on the figure. Values of the other circuit parameters are $R_A = 20\ \text{K}\Omega$, $C_A = 1\ \mu\text{F}$, $R_{BL} = 1\ \text{K}\Omega$, $C_{BL} = 5\ \mu\text{F}$, $R_s = 50\ \Omega$. These values were inserted into Eq. 13 or 14 to obtain the theoretical curves shown. The physiological range for A/ℓ is thought to be 0.1–1.0 (see text for discussion).

analysis: i.e., for the impedance results to differ detectably from those expected for the lumped model ($A/\ell = \infty$).

Is $A/\ell \leq 1$ cm likely for rabbit urinary bladder? Micrographs show that LIS width is near 100 Å, and that the cell diameter is $\sim 20\ \mu$. If we assume the cells to be cuboidal, then A/ℓ is calculated to be ~ 0.5 cm. for 1 cm^2 of epithelium.[1] Thus, distributed effects should be significant for rabbit urinary bladder, and our experimental results confirm this prediction (Fig. 5).

An alternative to impedance analysis with sinusoidal currents for the study of electrical circuits is transient analysis: measuring the circuit's voltage response to a square step of constant current. This is the experimental method used in most previous studies of epithelial impedance (Teorell and Wersall, 1945, Teorell, 1946, Rehm et al., 1976; Noyes and Rehm, 1970; Smith, 1975). Can a distributed circuit element be detected by transient analysis?

The voltage response of a circuit of linear RC elements to a step current input consists of sums of exponential functions whose amplitudes and time constants must be determined by curve fitting. If there is more than one time constant, the nonorthogonality of the exponential function makes this determination difficult and often impossible (Lanczos, 1956; Acton, 1970). However, there is still another difficulty. Consider the expression for the voltage response of the distributed circuit model (Fig. 1 *C*) to a square current step:

$$V(t) = \mathcal{L}^{-1}[Z_T \cdot (1/s)], \tag{16}$$

where Z_T is given by Eq. 13, $1/s$ is the Laplace transform of a unit step of current, the operator $\mathcal{L}^{-1}$ denotes the inverse Laplace transform, and $V(t)$ is the voltage response as a function of time. Fig. 3 depicts normalized $V(t)$ curves calculated for the same circuit parameter values and same four choices of A/ℓ used in Fig. 2. The curves are indistinguishable except for a slight deviation for $A/\ell = 0.01$, corresponding to an impossibly narrow LIS

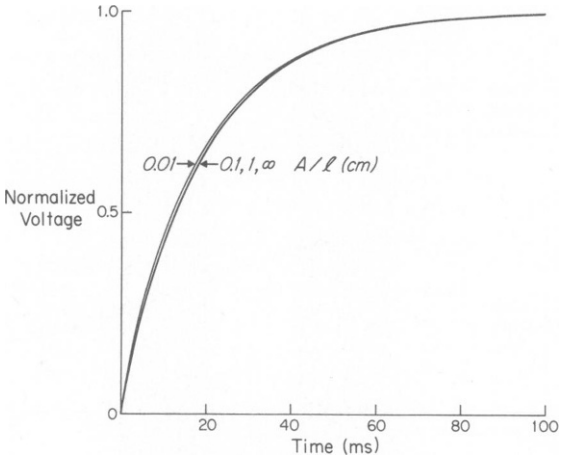

FIGURE 3 Effect of A/ℓ on the transient response computed as described in the text. A transient response is produced by applying a step of current and measuring the voltage response as a function of time. Ordinate: normalized voltage response—i.e., voltage normalized to the maximum steady-state voltage. The values of A/ℓ are shown on the figure. Values of the other circuit parameters are the same as those used in Fig. 2. Note that variation in A/ℓ produces negligible changes in the transient response, whereas it produces readily visible changes in the impedance graphs of Fig. 2.

width of 2 Å. Thus, transient analysis is unable to extract the morphological parameters of interest.[3] We have confirmed these conclusions by numerous computer simulations in which model parameters were chosen for the circuits of Figs. 1 *B* and 1 *C*, impedance and square-step responses were calculated, small random errors were added to these simulated data, and we then determined best-fit parameter values by the methods to be described in the section Analysis of Data. The best-fit parameter values extracted from simulated square-step data always deviated much further from the actual parameter values used to generate the data than did the best-fit parameter values extracted from simulated impedance data.

Why, for the same electrical circuit, is transient analysis so much less sensitive than impedance analysis for distributed effects? After all, one might reason, any wave form, including a square current pulse, can be described in terms of its Fourier integral as an infinite sum of sinusoidal currents of increasing frequency. Thus, it might seem that one is using the same test signal whether one applies these currents sequentially in impedance analysis or simultaneously in transient analysis. The explanation is that the two methods weight different frequencies very differently. Whereas impedance analysis weights frequencies equally, transient analysis preferentially weights low-frequency components: the frequency spectrum of a square step is such that the amplitudes of the sinusoids decrease hyperbolically with increasing frequency. But distributed effects, being basically series resistance effects, appear at middle to high frequencies. A step wave form simply does not contain enough of these frequencies to be sensitive to distributed effects.

[3] In Fig. 3 we show the normalized voltage response to a step input of current i.e., the voltage response divided by the steady-state voltage attained. The figure shows that there is a negligible change in the shape of the response, i.e., there is negligible deviation from a pure exponential (lumped) response. There is, however, a decrease in the apparent G_T with decrease in A/ℓ. We emphasize that this cannot be distinguished from a decrease in either of the membrane admittances.

METHODS

As a tight epithelium, we chose rabbit urinary bladder because its measured junctional resistance is effectively infinite ($\geq$300,000 Ω-cm^2: Lewis et al. 1976*b*). Dissection technique, chamber design, solution compositions, and microelectrode techniques were described previously (Lewis and Diamond, 1976, as modified by Lewis, 1977, and by Lewis et al., 1977). Briefly, the chamber design virtually eliminates edge damage by incorporating mounting rings with 20 pins to provide stable mounting, a flanged mounting bracket to eliminate lateral chamber movement, and use of Dow Corning vacuum grease as a sealant (Dow Corning Corp., Midland, Mich.). Exposed chamber area is 2 cm^2. The bladder is mounted vertically and impaled through chamber ports with a microelectrode slanting at ca. 60° with respect to the bladder. The chamber permits accurate temperature and pH control by well gassed baths. To assess edge damage, we noted for each preparation whether a point defined by the preparation's measured conductance (G_T) and short-circuit current (I_{sc}) fell below the mean G_T vs. I_{sc} relation in Fig. 16 of Lewis and Diamond (1976). If so, edge-damage conductance (G_{edge}) was estimated from the point's deviation from the relation. By computer simulation, we determined that a 10% paracellular shunt conductance ($G_{edge}/G_T = 0.1$) would cause only a 10% error in the determination of the other membrane parameters. In practice, G_{edge}/G_T was always much less than 0.1, due to the chamber design.

Transepithelial potential differences (PD's), whether spontaneous or caused by step or sinusoidal current, were measured with a high impedance differential voltage amplifier directly connected to Ag-AgCl electrodes mounted close to the preparation. Current was passed through a different set of Ag-AgCl electrodes further from the preparation and was measured by an operational amplifier (Teledyne Philbrick, Dedham, Mass.; model 1027) current-to-voltage converter. At high frequencies, the converter has significant input impedance that affects total current flow across the preparation. However, since transepithelial PD was measured differentially, and not with respect to the ground of the current amplifier, this input impedance did not affect impedance measurements.

Sinusoidal current for measuring impedance was generated by a Krohn-Hite oscillator (Krohn-Hite Corp., Avon, Mass.) and passed through a variable voltage divider and then through a 1 MΩ resistor to produce a relatively constant current. An accurate constant current source was not required, as both transepithelial PD and current were measured.

Impedance measurements were made by passing a small transepithelial sinusoidal current at different frequencies. The transepithelial voltage change ΔV and current were constantly monitored on an oscilloscope. ΔV was adjusted at each frequency to a level between 3 and 5 mV RMS. Both the current and voltage signals were amplified and filtered through phase-matched low pass filters (15 KHz, 60 db per octave roll-off) and led into the reference and signal inputs of a phase meter–RMS voltmeter. The output was displayed on a digital panel meter with integrating capability (for low frequencies) and printed on a digital printer. Magnitudes of voltage, current, and phase angle were printed for each frequency. The accuracy of the phase and magnitude measurements was better than 0.25° and 0.5%, respectively.

The preparation's impedance was measured in the range 2.2–10^4 Hz with six frequencies per decade (23 points). At the end of the run, duplicate points were taken at 10, 10^2, 10^3, and 10^4 Hz to verify that the preparation's response had not changed. A complete AC run took less than 15 min. Linearity was checked by doubling the current signal amplitude and verifying that impedance was independent of current amplitude.

The instrumentation was calibrated as follows. First, amplifier gain was verified to be constant by measuring the impedance of a carbon resistor (100 or 1,000 Ω) over the full frequency range. Second, the inherent phase shift (error) of the amplifiers and filters was measured repeatedly with a carbon resistor, verified to be constant for many months, and subsequently subtracted from the phase measured with the preparation in place. Finally, we verified that the complete set-up yielded expected impedance measurements for two artificial membranes, a Millipore filter (a "perfect" resistor) (Millipore Corp., Bedford, Mass.) and a piece of plastic wrap (a "perfect" capacitor in series with a small solution resistance). In both cases, after correction for the inherent phase error in the amplifiers, the phase angle remained constant at 0° and 90°, respectively, for the frequency range of interest, as expected.

We also routinely made the following measurements: I_{sc} as a measure of transport rate; spontaneous transepithelial PD, DC conductance (measured as the ratio of I_{sc} to spontaneous PD, and also measured by a DC current pulse); DC voltage-divider ratio α (ratio of basolateral to apical membrane conductances) measured by an intracellular microelectrode; and DC capacitance measured from the time constant of a square current step at high transepithelial resistance.

ANALYSIS OF DATA

All impedance data (phase angles and voltage and current magnitudes) were entered and stored on a digital computer (IBM model 360/91). The impedance was computed as the complex ratio of the voltage to the current. The inherent phase error of the instrumentation was then subtracted from the data to yield the corrected impedance.

To determine the circuit parameters of the preparation, we fitted the equivalent circuit model (Eq. 1 or 13) to the impedance data by means of a derivative-free nonlinear least-squares algorithm (Brown and Dennis, 1972) that minimizes the error between the theoretical curves and the experimental data by adjusting the parameter values of the theoretical curves. The actual computer routine (subroutine ZXSSQ) was implemented by International Mathematical and Statistical Libraries, Inc., Houston, Tex.

Both the phase angle and log magnitude (as a function of frequency) were simultaneously fitted. Each of these two curves, called the Bode plots, was normalized to its maximum value to weight the two plots equally. The more commonly used Nyquist or impedance locus representation, which plots imaginary versus real parts of the impedance with frequency as a parameter, has three disadvantages for our purposes: First, the phase angle is a much more sensitive indicator of changes in circuit values (Valdiosera et al., 1974*a*) than is a change in the real and imaginary parts. Second, the Nyquist plot represents magnitude of impedance linearly, hence giving high weight to low-frequency data because of their high values. Yet we maintain transepithelial voltage relatively constant across the preparation and allow capacitance current to reach high values, so that our magnitude measurements are accurate over the whole frequency range. The Bode plot's logarithmic representation of the magnitude is therefore preferable. Third, the differences between the lumped and distributed models of epithelia appear in the middle to high frequency range (cf. Fig. 2). These differences would be very difficult to resolve in a Nyquist representation, which lumps high frequency measurements in a small region near the plot origin.

Problems can arise when one attempts to adjust parameters that differ by several orders of magnitude: e.g., the total DC resistance is $\sim 10^4\ \Omega$, whereas the capacitor values are $\sim 10^{-6}$ F. Hence, we normalized parameter values to the initial estimates supplied to the fit algorithm.

Convergence to a minimum error was assumed when successive iterations during the minimization resulted in less than a 1% change in the parameter values. Given reasonable initial estimates of parameter values, convergence was usually accomplished within about 30 iterations of the fitting algorithm. The computer algorithm is specifically designed to avoid converging to so-called "false" or "local" minima. Nevertheless, we tested this frequently by providing different initial parameter estimates and verifying that the same set of best-fit parameters was determined for each case.

Our goal is to extract values of five parameters from impedance measurements by curve-fitting. In general, the number of parameters that can be meaningfully extracted from

data depends on the number and accuracy of measurements. How many parameters do our data warrant?

We followed the standard statistical test described by Hamilton (1964). For each curve-fit we computed Hamilton's R-factor, which expresses the percent misfit of theoretical curve to data. It is defined as:

$$R^2 = \frac{\sum_{i=1}^{n} [T(f_i, \beta_j) - E(f_i)]^2}{\sum_{i=1}^{n} E(f_i)^2},$$

where $T(f_i, \beta_j)$ are the theoretical predicted impedance values at frequency f_i when using the best-fit parameters β_j. $E(f_i)$ are the measured impedance. (The numerator of this expression is termed "the sum of the squares of the residuals".) Adding another variable, even a randomly chosen variable, to a theoretical equation must always result in a better (or at least as good a) fit to data. To determine whether the improvement in fit is due to a significant variable and exceeds the improvement expected for a randomly chosen variable, one calculates the ratio of R-factors of the two fits (with and without the added parameter). From the R-ratio, the number of parameters for each model, and the number of data points, one then uses a modified F-distribution to determine whether the added parameter is statistically significant. For example, we found that addition of an extra parameter to the lumped model to obtain the distributed model gave a highly significant improvement in fit for most bladders (see below, p. 311).

As an additional test of significance of extracted parameters, we calculated the standard deviation of each best-fit parameter from derivatives of the residuals function (difference between theoretical and experimental points) with respect to the parameter (Hamilton, 1964). If the standard deviation is an appreciable fraction of the parameter value itself, the parameter is poorly determined by the available data. We found this to happen when an added parameter produced an insignificant change in the best-fit curve as reflected by the R-ratio: e.g., when we attempted to extract C_{BL} in the absence of measurements of α (see third paragraph following).

In some cases, our impedance data were insufficient to determine unique values of all circuit parameters. A related problem arises when the mathematical best-fit occurs at a nonphysiological value of some parameter (e.g., a negative resistor value). These problems were handled either by allowing only a subset of the parameters to vary, while holding the others constant at assumed or independently measured values (e.g., by measuring α directly), or else by requiring parameter values to lie within the range of physiologically meaningful values (e.g., by constraining a parameter to remain positive and seeking the best-fit positive value).

In all cases, G_J was considered negligible compared to the membrane conductances on the basis of previous evidence for rabbit urinary bladder (Lewis et al., 1976*b*, 1977). Shunt conductance introduced by edge damage was also negligible due to improved mounting technique and chamber design, as already discussed under Methods.

Initially, we attempted to determine all six circuit parameters (R_A, R_S, A/ℓ, C_A; R_{BL} and C_{BL} determine through S_L/S_B as discussed above on p. 298) from impedance measurements alone. These attempts yielded physiologically unreasonable and poorly determined values of R_{BL} and C_{BL}. Electron micrographs show that basolateral membrane area is several times apical membrane area or exposed chamber area. Yet the extracted value of C_{BL} was only $\sim$0.1 μF for 2 cm^2 exposed area, with the nonsensical implication of only $\sim$0.05 cm^2 basolateral membrane per exposed cm^2. The extracted value of R_{BL}, $\sim$10 Ω, was equally nonsensical compared to directly measured values ($\sim$1000 Ω: Lewis et al., 1976*b*, 1977). In addition, standard deviations of extracted R_{BL} and C_{BL} values equalled or exceeded the values themselves, indicating poor determination of these parameters by the available data.

The cause of a failure of this sort could simply be that the two membrane time-constants are similar (i.e., differ by less than an order of magnitude). This would cause the two membrane impedances to combine mathematically to form effectively one impedance. The correctness of this explanation is shown by the fact that we had no difficulty extracting reasonable or independently confirmed values of all circuit parameters from impedance data alone in nystatin-treated rabbit bladders (see below, p. 313) or in frog gastric mucosa (Clausen, Machen, and Diamond; work in preparation) where the two time constants are known to be widely separated.

We dealt with this problem by directly measuring the voltage divider ratio α ($= R_A/R_{BL}$) by microelectrodes after each impedance run to determine independently the membrane DC resistances. Strictly speaking, α as measured by microelectrodes does not equal R_A/R_{BL}, but rather it equals R_A plus series resistance on the apical surface divided by R_{BL} plus series resistance on the basolateral surfaces. However, total series resistance is so low compared to R_A or R_{BL} in rabbit bladder that measured α may be equated with R_A/R_{BL}. We supplied this value to the curve-fitting procedure, which then determined circuit parameters subject to this constraint. This procedure yielded reasonable, well-determined values of all parameters.

RESULTS

Table II summarizes all parameter values obtained by fitting 34 impedance runs on 12 bladders to the lumped and distributed models. Four experimental conditions were used: basal transport in the absence of added agents (but there are large spontaneous differences among bladders in I_{sc}, as shown in Table II); stimulation of I_{sc} by adding 1 mM EGTA to the mucosal solution, thereby reducing free [Ca^{++}] and decreasing R_A (Lewis and Diamond, 1976); reduction of I_{sc} by adding 10^{-5} M amiloride to the mucosal solution; addition of nystatin to the mucosal or serosal solutions.

Table III gives the mean parameter values from the fits to the lumped and distributed models. This table utilizes 28 of the 34 experimental runs, omitting the six nystatin experiments plus experiment 31-1 (a bladder in which the spontaneous I_{sc} was an order of magnitude larger than usual). The nystatin results will be discussed at length later, and will not be considered in reporting the following mean parameter values unless specifically noted.

Area Measurements as Reflected by Capacitor Values

The average values of C_A extracted by the lumped and distributed models are virtually the same, 1.8 μF per cm^2 of chamber area, varying among individual preparations from 1.0 to 2.4

$\mu F/cm^2$. As biological membranes exhibit capacitances of ~ 1 μF per cm^2 of actual membrane area, the observed value means that there are 1.8 cm^2 of actual apical membrane area per cm^2 chamber area, i.e., that the epithelium and the apical membrane have only 80% more area than the nominal chamber area and are not highly folded. This conclusion is supported by micrographs (e.g., Fig. 1 of Lewis, 1977) which show the epithelium and apical membrane to be rather flat. (In contrast, in gastric mucosa we observe much higher values of C_A, correlated with prolific epithelial and membrane folding: Clausen et al., 1978). The modest variation of C_A among preparations probably reflects different degrees of stretch before mounting, a parameter that is difficult to reproduce exactly (low C_A means high stretch).

C_{BL} is on the average 4.9-fold higher than C_A: 6.5 ± 0.6 or 8.6 ± 0.8 ($n = 28$) μF per cm^2 chamber area, from the lumped or distributed model, respectively (see below, p. 312, for the reason for the difference). This C_{BL}/C_A ratio is in good agreement with micrographs, which show the cells to be can- or box-shaped with cell height roughly equal to diameter. A perfect cube would yield a C_{BL}/C_A ratio of 5: the apical membrane would correspond to the top of the cube, the basolateral membrane to the four sides and bottom. The range in C_{BL}/C_A calculated from impedance results is 2.5–12, indicating significant variation in cell shape among preparations. There is a significant inverse correlation between C_{BL} and G_T ($r = 0.67$, $p < 10^{-5}$ by a t-test), or between C_{BL} and I_{sc}. The reason for this trend is unclear; it is opposite to the trend that would arise as an artifact if there were microelectrode-induced damage to the apical membrane during α determinations (cf. Lindemann, 1975; Lewis et al., 1977).

Normalized Values of G_A, G_{BL}, I_{sc}, and R_s

Table IV gives values of G_A and G_{BL} normalized to the actual areas of these membranes by being expressed relative to C_A and C_{BL}, respectively (i.e., in units $\mu S/\mu F$). These normalized values can be approximately equated with values in units $\mu S/cm^2$, on the assumption that 1 μF corresponds to 1 cm^2 of actual membrane. We have also normalized I_{sc} and R_S to C_A as a measure of epithelial area, to correct for variation in degree of stretch of different preparations as discussed by Lewis and Diamond (1976).

G_A. Fig. 4 depicts the virtually linear relation between normalized G_A and normalized I_{sc} (experimental points ●). This relation, derived from impedance measurements, is similar to the relation deduced previously from two different techniques: a method based on use of nystatin to increase G_A (points ○ in Fig. 4, from Lewis et al., 1977); and direct-current measurements including voltage-divider ratios (Fig. 5 of Lewis et al., 1976*b*). The low value of the y-axis intercept (12 $\mu S/\mu F$) means that at moderate I_{sc} values the apical membrane approaches a Na^+ electrode, in the sense that G_A arises largely from the Na^+-specific transport-related entry channel. The asymptote represents a transport-unrelated conductance.

G_{BL}. In contrast to G_A, G_{BL} shows no significant correlation with I_{sc} ($p > 0.5$, $r = 0.046$ by linear regression and t-test), as already concluded by Lewis et al. (1976*b*). Averaging the results, we obtain an estimate for a previously unknown quantity, the value of G_{BL} normalized to basolateral membrane area: 120 $\mu S/\mu F$. Normalized instead to apical membrane area, this

TABLE IIA

PARAMETERS FOR INDIVIDUAL EXPERIMENTS FROM LUMPED MODEL

Expt	State	I_{sc}	R_T	α	SEM	No.	C_A	C_{BL}	R_S	R
		$\mu A/cm^2$	$K\Omega\text{-}cm^2$				$\mu F/cm^2$	$\mu F/cm^2$	$\Omega\text{-}cm^2$	%
31-1	Normal	57.	2.3	2.9	0.50	13	1.6	30.	17.	5.3
31-2	Amiloride	1.3	22.	17.	7.1	9	2.4	6.6	16.	4.6
32-1	Normal	0.80	37.	17.	2.5	19	1.3	4.5	23.	2.5
32-2	Amiloride	—	3.8	0.74	—	—	1.3	5.0	34.	3.0
33-0	Normal	2.6	23.	33.	2.3	40	1.3	7.4	17.	0.81
33-1	1 mM EGTA	3.8	16.	23.	1.4	—	1.4	7.1	12.	0.93
33-2	Amiloride	1.0	33.	33.	2.4	19	1.5	13.	12.	0.99
33-4	Mucosal nys.	—	2.3	1.1	—	—	1.5	24.	12.	1.6
33-5	Serosal nys.	—	12.	170.	—	—	1.8	9.5	19.	2.3
34-1	Normal	1.1	42.*	26.	1.9	24	1.0	3.4	15.*	6.3
34-2	1 mM EGTA	2.7	21.	11.	0.90	29	1.2	3.1	32.	2.4
34-3	Amiloride	1.1	31.	23.	4.1	16	1.3	4.6	37.	2.6
35-1	Normal	2.6	18.	28.	3.7	23	1.7	7.0	22.	1.9
35-2	1 mM EGTA	3.6	16.	13.	1.4	15	1.9	5.5	15.	1.8
35-3	Amiloride	0.65	22.	24.	4.1	12	1.9	6.3	16.	2.1
36-1	Normal	1.9	19.	25.	2.9	30	1.3	5.3	36.	2.6
36-2	1 mM EGTA	6.0	7.9	7.9	2.4	—	1.9	4.2	31.	2.6
37-1	Normal	2.6	18.	19.	1.2	12	2.3	12.	24.	2.4
37-2	Amiloride	1.0	28.	16.	1.9	31	2.4	8.9	28.	3.8
37-3	Mucosal nys.	—	2.0	1.5	—	—	1.8	27.	34.	4.8
38-1	Normal	1.6	28.	22.	2.1	18	1.3	4.5	13.	4.0
39-1	Normal	1.9	25.	16.	1.2	17	1.5	5.0	28.	3.6
39-3	Amiloride	0.55	36.*	13.	3.2	7	1.7	4.3	22.	5.3*
40-1	Normal	2.0	27.	25.	2.8	16	1.7	8.2	17.	2.0
40-2	1 mM EGTA	4.7	24.	18.	1.8	16	1.9	7.3	14.	2.7
40-3	Amiloride	1.7	25.	30.	3.2	12	2.0	8.3	16.	2.7
40-4	1 mM EGTA	5.0	13.	12.	0.60	12	2.2	7.1	14.	2.8
40-5	Mucosal nys.	—	0.75	1.2	—	—	1.6	28.	9.0	6.5
41-1	Normal	2.3	20.	7.0	0.40	15	1.7	4.0	29.	1.3
41-2	1 mM EGTA	4.8	13.	3.7	0.40	7	2.2	3.4	28.	1.2
41-3	Amiloride	1.4	32.	8.8	0.90	21	2.0	5.8	27.	1.4
42-1	Normal	11.	7.1	3.0	0.20	7	1.9	18.	2.5	4.2
42-2	1 mM EGTA	11.	8.4	2.6	0.20	6	1.9	1.5	19.	2.9
42-3	Amiloride	0.44	29.	8.9	0.90	9	2.4	5.4	22.	3.2
Mean CV			0.026				0.020	0.11	0.023	
SD			0.014				0.11	0.22	0.011	

This table shows the results of the curve fits using the lumped model to the 34 experimental runs described in the paper. The values presented are for 1 cm^2 of preparation; they are not normalized to membrane capacitance.

The first column (Expt) identifies the actual impedance run. The first number is the preparation number, whereas the second number is the run number (i.e., 33-0, 33-1, 33-2, etc., are all from the same bladder). The second column (State) gives the added agent, if any ("normal" = no added agent; "nys." = nystatin).

I_{sc} and α values were measured directly, except that α was extracted from fits in runs 32-2, 33-4, 33-5, 37-3, and 43-1. Values of other parameters are fitted ones. Standard error of the mean (SEM) and number of measurements (No.) are given for measured α values. R is the Hamilton R-factor, and can be interpreted as the percent misfit of the model to the data.

The last two rows of the table give the mean value and standard deviation for the coefficient of variation of the fitted parameters. These were determined by averaging each parameter's coefficient of variation (defined as the standard deviation of the best-fit parameter divided by the parameter value itself; estimated parameter standard deviations were estimated by the method of Hamilton, as discussed above, p. 000).

*Indicates parameter values where the coefficient of variation lies outside two standard deviations from the mean of the coefficients of variation for all experiments.

TABLE IIB

PARAMETERS FOR INDIVIDUAL EXPERIMENTS FROM DISTRIBUTED MODEL

Expt	R_T	α	SEM	No.	C_A	C_{BL}	R_S	A/ℓ	R	R-ratio
	$K\Omega$-cm^2				$\mu F/cm^2$	$\mu F/cm^2$	Ω-cm^2	cm	%	
31-1	2.9	2.9	0.50	13	2.0	34.	12.	0.15	2.5	2.1
31-2	21.	17.	7.1	9	2.4	11.	12.	0.32	2.1	2.2
32-1	36.	17.	2.5	19	1.4	5.2	18.	0.55	1.3	1.9
32-2	3.8	1.1	—	—	1.3	8.1*	28.	0.53	0.85	3.6
33-0	23.	33.	2.3	40	1.3	7.5	16.	(86.)	0.81	1.0†
33-1	16.	23.	1.4	—	1.4	7.2*	10.	(7.2)	0.91	1.0†
33-2	33.	33.	2.4	19	1.5	14.	10.	(6.4)	0.92	1.1†
33-4	2.3	1.1	—	—	1.5	24.	11.	(11.)	1.6	1.0†
33-5	12.	58.	—	—	1.9	11.	15.	(1.4)	1.7	1.3
34-1	41.*	26.	1.9	24	0.99*	5.8*	9.0*	0.25	3.5	1.8
34-2	21.	11.	0.90	29	1.2	3.5	27.	0.45	1.4	1.8
34-3	31.	23.	4.1	16	1.3	5.8	31.	0.46	1.0	2.6
35-1	18.	28.	3.7	23	1.7	8.4	17.	0.99	1.4	1.4
35-2	16.	13.	1.4	15	1.9	5.9	12.	1.2	1.5	1.2
35-3	22.	24.	4.1	12	1.9	7.2	12.	0.85	1.3	1.7
36-1	19.	25.	2.9	30	1.3	7.4	29.	0.51	0.92	2.8
36-2	7.8	7.9	2.4	—	1.9	5.0	26.	0.36	0.85	3.0
37-1	17.	19.	1.2	12	1.8	21.	19.	0.70	0.65	3.7
37-2	27.	16.	1.9	31	2.4	15.	23.	0.30	0.98	3.9
37-3	1.9	1.5	—	—	2.3	34.	29.	0.096	3.2	1.5
38-1	27.	22.	2.1	18	1.3	5.6	7.8	0.52	1.8	2.2
39-1	24.	16.	1.2	17	1.4	6.8	22.	0.44	1.4	2.5
39-3	34.*	13.	3.2	7	1.6	8.0	16.	0.22	2.7	2.0
40-1	27.	25.	2.8	16	1.7	10.	13.	1.0	0.94	2.1
40-2	14.	18.	1.8	16	1.9	9.4	9.4	0.77	0.75	3.5
40-3	25.	30.	3.2	12	2.0	11.	11.	0.76	1.1	2.5
40-4	12.	12.	0.60	12	2.2	9.5	9.4	0.58	0.86	3.2
40-5	0.60	1.4	—	—	2.1*	59.	5.6	0.10	4.1	1.6
41-1	20.	7.0	0.40	15	1.7	4.1	26.	1.9	1.2	1.1
41-2	13.	3.7	0.40	7	2.2	3.4	26.	0.34	0.99	1.3
41-3	32.	8.8	0.90	21	2.1	5.9	24.	1.5	1.1	1.2
42-1	6.8	3.0	0.20	7	2.2	16.	21.	0.21	0.81	5.2
42-2	8.3	2.6	0.20	6	2.0	15.	15.	0.63	0.98	3.0
42-3	28.	8.9	0.90	9	2.4	6.4	19.	0.27	1.3	2.4
Mean CV	0.0123				0.0096	0.065	0.0119	0.135		
SD	0.0076				0.0055	0.054	0.0063	0.171		

This table is as Table IIa, except that it shows the results of the curve fits using the distributed model (rather than the lumped model) to the 34 experimental runs described in the paper. The experimental state and I_{ss} values for each run can be found in the corresponding row of Table IIa.

The last column of the table (R-ratio) shows the Hamilton R-ratio; it is the ratio of the R-factor of the distributed model to that of the lumped model. The R-ratios can be interpreted as the improvement of fit of the distributed model over the lumped model (e.g., an R-ratio of 2.1 means that the residual-misfit error of the distributed model is 2.1 times less than that obtained by the fit to the lumped model). The degrees of freedom (number of experimental data points minus number of parameters determined by curve fitting) were between 40 and 49 for all experiments.

Given the R-ratio and the degrees of freedom, we computed the probability that the added parameter in the distributed model is not statistically significant (see text).

†$P > 0.005$: i.e., in these cases, the distributed model does not significantly improve the fit, hence the A/ℓ values (set in parentheses) should be considered too large to determine meaningfully.

TABLE III
AVERAGE CIRCUIT PARAMETERS

	Mean	Standard error
Lumped Model		
C_A ($\mu F/cm^2$)	1.8	0.1
C_{BL} ($\mu F/cm^2$)	6.5	0.6
C_{BL}/C_A	3.8	0.4
R_s (Ω-cm^2)	22.	7.4
R-factor (%)	2.7	0.3
Distributed Model		
C_A ($\mu F/cm^2$)	1.8	0.1
C_{BL} ($\mu F/cm^2$)	8.6	0.8
C_{BL}/C_A	4.9	0.4
R_S (Ω-cm^2)	18.	1.
R-factor (%)	1.3	0.1
Normalized Parameters—Distributed Model		
G_{BL} ($\mu S/\mu F$) (normalized to C_{BL})	120.	11.
R_S (Ω-μF) (normalized to C_A)	31.	3.
A/ℓ (cm/μF) (normalized to C_A)	0.34	0.04

This table shows average values of several circuit parameters from the data of Table II. The five nystatin runs and experiment 31-1 were not included in computing these average values. In addition, the mean value of A/ℓ was computed only from those runs where the improved fit of the distributed over the lumped model was significant at the $P < 0.005$ level (i.e., this added parameter A/ℓ was highly statistically significant). For all parameters except A/ℓ, the population size (n) was 28. For A/ℓ, n was 24.

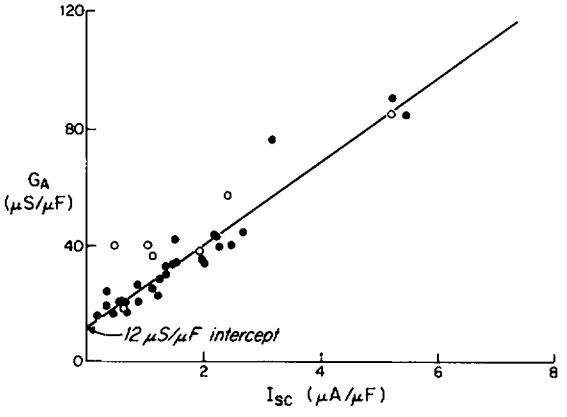

FIGURE 4 Relationship between apical conductance (G_A) and Na^+ transport rate of the tissue (as reflected by the short circuit current, I_{sc}), both normalized to apical capacitance. Experimental points (•) are taken from Table IV, omitting the six runs mentioned in the legend of Table III. The line is the best-fit straight line through the data: $G_A = 12\ \mu S/\mu F + (I_{sc})(14\ \mu S/\mu F)$ ($r = 0.96$, $n = 28$). Points ○ are from measurements by Lewis et al. (1977), based on the use of nystatin and corrected for underestimation of C_A as described in the text. These data show the good agreement between the nystatin method described by Lewis et al. and the impedance methods developed in the present paper.

TABLE IV

PARAMETERS NORMALIZED TO MEMBRANE CAPACITANCES

Expt	State	I_{sc}/C_A	G_T/C_A	G_A/C_A	G_{BL}/C_A	G_{BL}/C_{BL}	$R_S C_A$	$(A/\ell)/C_A$	C_{BL}/C_A
		$\mu A/\mu F$	mS/μF	mS/μF	mS/μF	mS/μF	Ω-μF	cm/μF	
31-1	Normal	29.	0.23	0.30	0.051	0.87	24.	0.078	17.
31-2	Amiloride	0.55	0.020	0.021	0.081	0.36	28.	0.14	4.4
32-1	Normal	0.59	0.020	0.021	0.094	0.36	24.	0.41	3.9
32-2	Mucosal nys.	—	0.20	0.38	0.068	0.41	37.	0.40	6.1
33-0	Normal	2.0	0.033	0.034	0.20	1.1	21.	(66.)	5.7
33-1	1 mM EGTA	2.7	0.043	0.045	0.21	1.0	15.	(5.0)	5.0
33-2	Amiloride	0.66	0.020	0.021	0.077	0.69	16.	(4.2)	8.9
33-4	Mucosal nys.	—	0.28	0.53	0.038	0.61	17.	(7.4)	16.
33-5	Serosal nys.	—	0.044	0.045	0.43	2.6	29.	0.72	6.0
34-1	Normal	1.1	0.024	0.025	0.11	0.66	9.0	0.26	5.9
34-2	1 mM EGTA	2.2	0.040	0.043	0.17	0.48	34.	0.37	2.8
34-3	Amiloride	0.86	0.026	0.027	0.13	0.61	39.	0.36	4.6
35-1	Normal	1.5	0.033	0.034	0.19	0.96	29.	0.59	4.9
35-2	1 mM EGTA	2.0	0.033	0.035	0.15	0.46	22.	0.63	3.2
35-3	Amiloride	0.34	0.023	0.024	0.16	0.60	24.	0.44	3.7
36-1	Normal	1.5	0.040	0.042	0.19	1.1	39.	0.39	5.6
36-2	1 mM EGTA	3.2	0.068	0.076	0.23	0.61	50.	0.19	2.7
37-1	Normal	1.5	0.032	0.034	0.054	0.64	35.	0.39	12.
37-2	Amiloride	0.44	0.016	0.017	0.041	0.27	55.	0.13	6.5
37-3	Mucosal nys.	—	0.24	0.39	0.040	0.60	67.	0.042	15.
38-1	Normal	1.2	0.027	0.029	0.15	0.63	10.	0.39	4.2
39-1	Normal	1.3	0.028	0.030	0.11	0.50	32.	0.30	4.7
39-3	Amiloride	0.34	0.018	0.020	0.050	0.25	26.	0.13	5.0
40-1	Normal	1.2	0.022	0.023	0.095	0.57	22.	0.60	6.0
40-2	1 mM EGTA	2.5	0.038	0.040	0.14	0.71	18.	0.40	4.9
40-3	Amiloride	0.88	0.020	0.021	0.12	0.62	22.	0.38	5.3
40-4	1 mM EGTA	2.3	0.037	0.040	0.11	0.48	21.	0.26	4.3
40-5	Mucosal nys.	—	0.79	1.4	0.066	1.9	12.	0.049	28.
41-1	Normal	1.3	0.029	0.033	0.097	0.23	45.	1.1	2.4
41-2	1 mM EGTA	2.2	0.034	0.044	0.11	0.16	57.	0.15	1.5
41-3	Amiloride	0.68	0.015	0.017	0.053	0.15	50.	0.74	2.9
42-1	Normal	5.2	0.068	0.091	0.037	0.27	47.	0.097	7.5
42-2	1 mM EGTA	5.5	0.061	0.085	0.030	0.22	29.	0.32	7.5
42-3	Amiloride	0.18	0.015	0.016	0.054	0.14	46.	0.11	2.6

This table shows values of circuit parameters normalized to membrane areas as reflected by membrane capacitances. The data are taken from fits to the distributed model shown in Table II*b*. A/ℓ values enclosed in parentheses are not significant, as determined by the Hamilton *R*-ratio test.

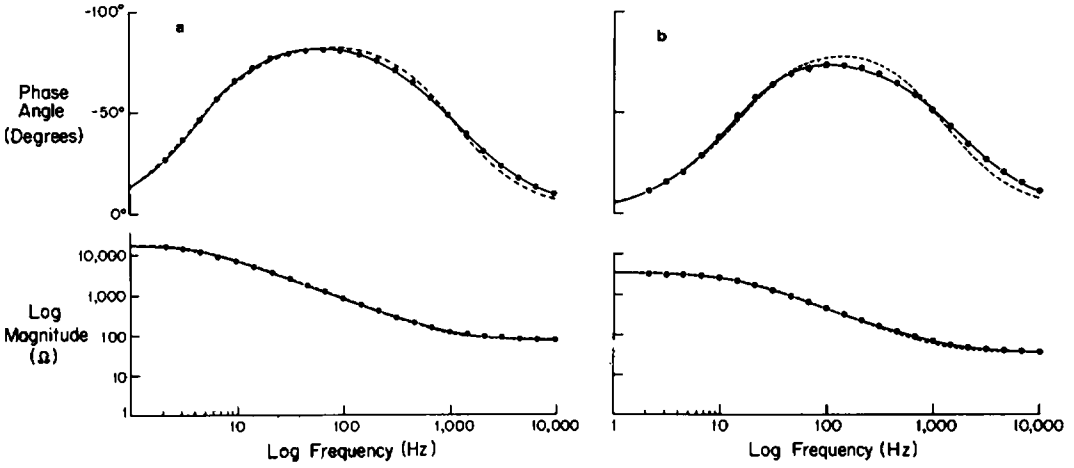

FIGURE 5 Results of curve-fitting the measured impedance of normal preparations. Left (*a*), experiment 37-1; right (*b*), experiment 42-1. Points • are the measured impedance, the broken line is the fit to the lumped model, and the solid line is the fit to the distributed model. The resulting best-fit parameter values can be found in Table II for experiments 37-1 and 42-1. The deviations seen in fitting the lumped model are typical: the measured phase angle is generally overestimated in the mid frequency range and underestimated in the high frequency range. Also noted that the differences between the two models show up mostly in the phase curve (above), and the impedance magnitude curve (below) is not sensitive to these effects.

becomes 570 μS/μF. Lewis et al. (1977) used nystatin to short out R_A and thereby could directly measure G_{BL} (normalized to C_A) as 790 μS/μF. Their step-response method of reestimating C_A probably underestimated it by about 20% (Lewis et al., 1976*a*), so that their value should be corrected to (790)(0.8) = 630 μS/μF, agreeing with our value of 570 derived from impedance measurements.

R_S. The resistance measured between our two voltage electrodes after removing the bladder averages 48 Ω-cm^2. This represents the bulk solution between the two voltage-recording electrodes. Yet the value of R_S extracted from impedance analysis with the bladder in place is 66 Ω-cm^2 ($\pm$ 1.3, n = 28; Table III). The difference of 66 − 48 = 18 Ω-cm^2, or 31 Ω-μF (related to apical membrane area), must arise from tortuosity and reduced ionic mobility in the unstirred layers constituted by bladder connective tissue and nontransporting cell layers. Here we treat these series resistances as a pure resistor, but there may be conditions where a reactive component (capacitance) cannot be ignored (see below, p. 315).

The Distributed Effect

Figs. 5 *a* and 5 *b* compare the fits of the distributed model and the lumped model to two typical sets of impedance measurements, experiments 37-1 and 42-1. For phase-angle measurements (Figs. 5 *a* and 5 *b*, upper curves) the lumped model fits the data only up to about 50 Hz and predicts too high values at middle frequencies and too low values at high frequencies, whereas the distributed model gives a good fit over the whole frequency range. Impedance magnitude measurements scarcely discriminate between the two models (Figs. 5 *a*

and 5 *b*, lower curves). The same misfits[4] of the lumped model to phase angle measurements were observed in 24 of the 28 nonnystatin experiments in Table II. The reason for the absence of misfit in the other four experiments will become apparent below.

We interpret the distributed resistor as arising from the relatively long and narrow lateral spaces. Four observations support this conclusion:

(1) In our interpretation, the extra parameter associated with the distributed model is A/ℓ, the ratio of cross-sectional area to length of the lateral spaces. This parameter is a function of the amount of preparation exposed in the chamber and must somehow be normalized to account for variation in this amount among preparations, due to variation in stretch. Normalized to apical capacitance, the mean fitted value of A/ℓ is 0.34 ± 0.04 cm/μF (n = 24). Equating 1 μF apical capacitance with ~1 cm^2 actual membrane area, and assuming cells to be smooth cubes 20 μ on a side, this A/ℓ value yields a lateral space width of 68 Å. The width seen in electron micrographs of mammalian urinary bladders (mostly mouse, no detailed studies for rabbit) is around 100 Å. This agreement is remarkable when one considers that the former value is derived from electrical rather than morphological measurements.

The limit of resolution of A/ℓ in our experiments is ~1 cm/μF: i.e., larger values of A/ℓ mean that distributed effects were too small for us to resolve significantly.

(2) In three impedance runs on one bladder (Fig. 6), the lumped model gave an excellent fit to the data, the fit of the distributed model was indistinguishable to the eye, both fits gave

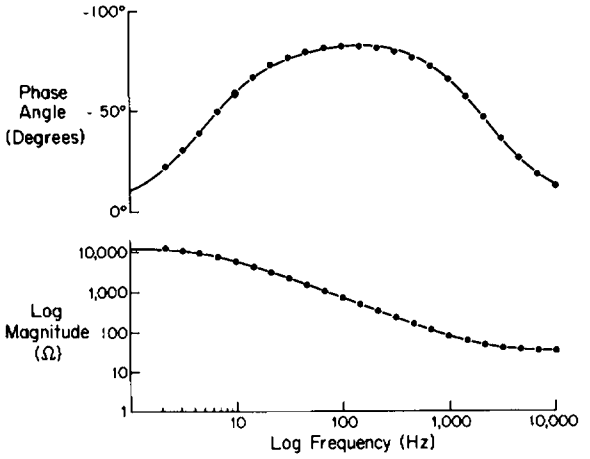

FIGURE 6 Measured impedance values for the highly stretched bladder of experiment 33-0 (see Table II for best-fit parameter values). The line through the data is the fit to the lumped model, from which the fit to the distributed model cannot be distinguished. The good fit by the lumped model is due to the high degree of stretch in this preparation, thereby increasing the parameter A/ℓ and eliminating the distributed effect (see text for discussion).

[4]In these 24 experiments, the improved fit of the distributed model over the lumped model was significant at least at the $p < 0.005$ level, on the average at the $p < 10^{-6}$ level, often at much higher levels, by the Hamilton test. Thus, the one extra parameter of the distributed model is not just a minor quantitative correction, but rectifies qualitatively consistent misfits and has strong statistical support. Expressed another way, the distributed model fits the data twice as well as the lumped model (R-factor or percent misfit 1.3 and 2.7%, respectively).

the same R-factor (0.81%), and the extra parameter of the distributed model was not statistically significant. What distinguished this bladder is that it was greatly stretched before mounting. This would tend to decrease the length or increase the area of the lateral spaces, increasing A/ℓ and hence causing the distributed model to reduce to the lumped model (see derivation of Eq. 14 from Eq. 13).

(3) Agents that cause the cells to swell might be expected to compress the lateral spaces and decrease A/ℓ, making the distributed effect more noticeable. Such an agent is the polyene antibiotic nystatin, which greatly increases bladder cation conductance (see below) and thereby causes gross cellular swelling visible in a dissecting microscope. In the stretched bladder, which exhibited no distributed effect (Fig. 6), addition of nystatin at 120 units/ml to the serosal solution produced the following results: α increased from 23 to 110, due to the increased conductance of the serosal membrane; the lumped model no longer fitted the impedance measurements; instead, the distributed model was required, suggesting compression of the lateral spaces by cell swelling.

(4) In almost all experiments, the value of C_{BL} extracted from the distributed model exceeded that from the lumped model (on the average, by 68 $\pm$ 3%, $n = 24$). This difference arises because the distributed resistor of the lateral spaces reduces current flow across the portion of the lateral membrane nearest the mucosal solution, an effect ignored in the lumped model.

While the lateral spaces themselves are physiologically important for bladder transport, the distributed effect is not physiologically significant. Its significance is rather that neglect of it may cause membrane capacitances measured by impedance or step transient methods to be seriously in error.

Effects of Added Agents

One goal of impedance analysis is to localize effects of agents on the bladder: e.g., to identify whether an agent that increases bladder permeability does so by increasing membrane area (reflected in increased C_A or C_{BL}) or by altering existing membrane conductances (reflected in a change in normalized R_A or R_{BL}), and whether the effect is on the apical or basolateral membrane. To validate this approach, we measured impedance before and after exposure of bladders to three agents whose mechanism of action was already shown.

EGTA. Removal of Ca^{++} from the mucosal solution, either by using Ca^{++}-free solutions or by buffering with EGTA, stimulates I_{sc} and increases G_T (Curran and Gill, 1962; Cuthbert and Wong, 1972; Lewis and Diamond, 1976). Lewis and Wills (data in preparation) showed that this increase in G_T arose largely from an increase in G_A, but that EGTA also had other effects. In eight experiments (Tables II and IV) we obtained impedance runs on bladders before and after application of EGTA, and extracted values of membrane parameters. Increases in G_T and I_{sc} occurred in six of these eight EGTA runs. In all six cases the extracted value of G_A increased. Changes in other parameters were smaller or inconsistent.

Amiloride. Lewis et al. (1976*b*) showed that amiloride blocks Na^+ transport in rabbit urinary bladder by reducing G_A. Tables II and IV summarize the results of nine impedance experiments with amiloride. In all cases, I_{sc} and G_T decreased, as found previously. Of the membrane G and C values extracted by fitting the impedance data, the only one that changed

significantly or consistently was G_A, which decreased in all nine experiments (on the average, from 35 to 25 $\mu S/\mu F$).

Nystatin. Lewis et al. (1977) showed that addition of nystatin to the mucosal solution increases bladder conductance by increasing cation conductance of the apical membrane. Choosing a nystatin dose that yields sufficiently stable conductance changes for impedance analysis is a tricky problem: low doses produce negligible changes because of nystatin's very steep dose-response curve (Fig. 7 of Lewis et al., 1977), while high doses cause cell swelling and eventually lysis. Hence we adopted a compromise procedure of Lewis et al. (1977): nystatin was added to the mucosal solution to a level of 120 units/ml, G_T was monitored by square pulses, and the mucosal solution was rapidly flushed with nystatin-free solution as soon as G_T began to rise. This increases membrane conductance but not to a level causing cell lysis. Nystatin washout from bladder membranes is sufficiently slow ($t_{1/2} \sim 40$ min, as judged by G_T changes) that G_T is virtually constant during the time required for impedance measurements from 10 to 10^4 Hz ($\leq$3 min).

Fig. 7 depicts impedance measurements for such a nystatin-treated bladder, for comparison with measurements on the same bladder before nystatin. The most striking change in a parameter value caused by nystatin was in G_A, which increased from 21 to 380 $\mu S/\mu F$. For the nystatin-treated bladder, it was possible to obtain a unique curve-fit without supplying α measurements to the computer, and the extracted α value (1.1) agrees reasonably with the measured value (1.9), based on a single microelectrode penetration. This agreement contrasts with the difficulty in curve-fitting normal bladders with their high α's ($\sim$30), unless a measured α value was supplied to the computer (see p. 304 and p. 315 for discussion).

In three other bladders exposed to mucosal nystatin, G_T and G_A similarly increased 10–35-fold, while G_{BL} and C_A showed little change. The extracted C_{BL} value increased fourfold; this apparent change may not be real (see p. 315 for discussion).

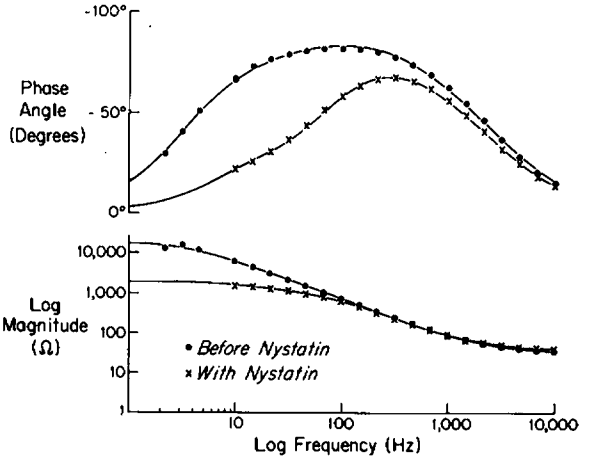

FIGURE 7 Fit to impedance data measured before (experiment 32-1, points •) and after (experiment 32-2, points ×) application of 120 units/ml of nystatin on the apical side. See Tables II and IV for best-fit membrane parameter values. The solid lines through the data are the fits to the distributed model (the fits to the lumped models are not shown).

DISCUSSION

Adequacy and Sensitivity of Impedance Measurements

If one's goal is to make measurements that would extract values of all depicted circuit elements for an epithelium that is adequately represented by the equivalent circuit of Fig. 1 *B* or 1 *C*, steady-state DC measurements cannot succeed, even in principle. Transient DC transepithelial measurements can succeed in principle (if $G_J = 0$), but rarely in practice, because determination of not too widely-spaced exponential time-constants requires data of an accuracy unattainable in physiological experiments. Transepithelial impedance measurements can sometimes achieve this goal. However, it is important to realize that, in at least two situations, even impedance measurements may not permit complete determination of the circuit without additional information.

One such situation occurs when G_J is not negligible, i.e., if the epithelium is leaky. Then the impedance of the circuit of Fig. 1 *B* (omitting R_S for simplicity) is described by the following ratio of two polynomials in the Laplace transform variable s ($= j\omega$ for the sinusoidal steady state):

$$Z_T = \frac{1}{C_A + C_{BL}} \cdot \frac{s(C_A + C_{BL}) + G_A + G_{BL}}{s^2 C_A C_{BL} + s[C_A(G_{BL} + G_J) + C_{BL}(G_A + G_J)] + G_A(G_{BL} + G_J) + G_{BL}(G_A + G_J)}.$$

This is an equation of the form: $Z_T = (s + A)/(Bs^2 + Cs + D)$, which is fully described by only four parameters, A, B, C, and D. Yet the circuit has five elements: G_A, G_{BL}, G_J, C_A, and C_{BL}. Hence it is impossible for any curve-fitting procedure based on transepithelial impedance measurements alone to extract all five of these elements for a leaky epithelium. Some additional measurements, such as determination of α as a function of frequency by AC microelectrode techniques, are required.

A second situation is that available impedance measurements may not suffice in practice for determination of all circuit elements. This problem may arise from insufficiently precise data, insufficiently numerous data, or relative insensitivity of the fitted curve to the value of one or more parameters. Then alternative sets of parameters differing widely in the value of one or more parameters may fit the data equally well. Rabbit urinary bladder provides an example: the apical membrane has a higher resistance compared to the basolateral membrane; however, it has a smaller relative area and hence smaller capacitance. This results in similar time constants for the two membranes and makes determination of the membrane impedances (from transepithelial impedance only) difficult. We had to resort to independent measurements of α to determine R_A/R_{BL} and hence separate the membrane impedances. This was not needed, however, in nystatin-treated bladders, where the apical membrane time constant was sufficiently short compared to the basolateral time constant.

Choice of Model

For equivalent circuit analysis to be meaningful, the analysis must be based on an accurate, morphologically realistic circuit model. The circuit will generally contain morphological

parameters, whose values might therefore be extracted from electrical measurements on live epithelia. Since epithelia differ in morphology, they may also differ in appropriate equivalent circuit. For example, the distributed effect in rabbit urinary bladder arises at the basolateral membrane, but a different model is required for gastric mucosa, where a very large distributed effect arises from the tubulovesicular system in the apical membrane (Clausen et al., 1978).

In the case of rabbit urinary bladder, we found the lumped model of Fig. 1 *B* to be adequate only for highly stretched preparations. Normally the lumped model gave a misfit that was sufficiently improved by addition of one morphological parameter to yield the distributed model of Fig. 1 *C*. Even Fig. 1 *C* is obviously highly schematic, especially in that it treats the two nontransporting cell layers at the serosal side of the preparation simply as a series resistance. Usually the apical membrane impedance of the transporting cell layer so dominates the total impedance that the reactive (capacitative) impedance of the nontransporting layers may be neglected. However, this condition no longer applies when apical impedance is greatly decreased by nystatin. This simplification in the circuit of Fig. 1 *C* may perhaps be the reason why that circuit gave a poor fit, with high C_{BL} values, to impedance data from some nystatin-treated bladders.

Validation of Impedance Analysis for Rabbit Urinary Bladder

The goal of this paper has been to validate our methods of impedance analysis for rabbit urinary bladder by showing that the methods yield results confirmed by independent techniques. The evidence for validity of the method is as follows:

(1) The extracted C_A is 1.8 μF per cm^2 exposed chamber area, agreeing with microscopic observations that the epithelium is not folded and that the apical membrane lacks microvilli. If the apical surface were perfectly smooth, one would expect $C_A \sim 1$ μF/cm^2. In contrast, impedance analysis of gastric mucosa, a grossly folded epithelium with a highly invaginated apical surface, yields extracted C_A values in excess of 650 μF/cm^2 (Machen et al., 1977).

(2) The extracted C_{BL}/C_A ratio is 4.9, agreeing with the value of $\sim$5 expected for the cuboidal cell shape as seen in micrographs.

(3) In the one situation where we were able to extract α from impedance data (in a nystatin-treated bladder), the extracted value of 1.1 agreed reasonably with a single measurement of 1.9 by DC microelectrode techniques.

(4) The extracted G_{BL} value is 570 μS per μF of apical capacitance, agreeing with the value of 630 μS/μF that Lewis et al. (1977) measured by shorting out the apical membrane with nystatin.

(5, 6) The extracted G_A value varies linearly with, and the extracted G_{BL} is independent of, I_{sc} (Fig. 5), as Lewis et al. (1976*b*) found by cable analysis and other DC methods.

(7) The distributed effect observed in normal bladders yields a lateral space width of 68 Å, close to the value of $\sim$100 Å estimated from electron micrographs. The distributed effect disappears in stretched bladders but reappears after nystatin treatment, as one might expect from anticipated changes in lateral space length or width.

(8) The principal changes in extracted circuit parameters of bladders treated with mucosal EGTA, mucosal amiloride, mucosal nystatin, and serosal nystatin are, respectively, an increase in G_A, decrease in G_A, increase in G_A, and increase in G_{BL}. These conclusions agree with those obtained by other techniques (Lewis et al., 1976*b*, 1977).

These validations of numerous results of impedance analysis by other techniques mean that the impedance methods we have developed for rabbit urinary bladder may now be trusted to study unsolved problems in this preparation.

We acknowledge with pleasure the help of: A. Peskoff for suggestions in deriving the distributed model; R. S. Eisenberg and R. T. Mathias, in the initial experimental design; D. C. Eaton, in providing useful discussions and the facilities of his laboratory where some of the experiments were performed; and T. E. Machen, who offered helpful suggestions.

This work was supported by National Institutes of Health grants GM 14772, AM 17328 (UCLA Center for Ulcer Research and Education), and AM 20851. Computer time was provided by the UCLA Campus Computing Network. Dr. Clausen was a predoctoral fellow at the Center for Ulcer Research and Education.

Received for publication 24 August 1978 and in revised form 28 November 1978.

REFERENCES

ACTON, F. 1970. Numerical Methods that Work. Harper & Row, Publishers, Inc. New York. 252–253.

BROWN, A. C., and K. G. KASTELLA. 1965. The AC impedance of frog skin and its relation to active transport. *Biophys. J.* **5**:591.

BROWN, K. M., and J. E. DENNIS, JR. 1972. Derivative free analogues of the Levenberg-Marquardt and Gauss algorithms for nonlinear least squares approximation. *Numer. Math.* **18**:289.

CLAUSEN, C., J. M. DIAMOND, and T. E. MACHEN. 1978. Electrical events that accompany HCl production in gastric mucosa. *Biophys. J.* **21**:169*a*. (Abstr.).

COLE, K. S. 1972. Membranes, Ions, and Impulses. University of California Press, Berkeley, Calif. 12.

CURRAN, P. F., and J. R. GILL. 1962. The effect of calcium on sodium transport by frog skin. *J. Gen. Physiol.* **45**:625.

CUTHBERT, A. W., and P. Y. D. WONG. 1972. The role of calcium ions in the interaction of amiloride with membrane receptors. *Mol. Pharmacol.* **8**:222.

DAVSON, H. 1964. A Textbook of General Physiology. Little, Brown and Company, Boston, Mass. 681.

EISENBERG, R. S., and E. A. JOHNSON. 1970. Three-dimensional electrical field problems in physiology. *Prog. Biophys. Mol. Biol.* **20**:1.

FALK, G., and P. FATT. 1964. Linear electrical properties of striated muscle fibres observed with intracellular electrodes. *Proc. Roy. Soc. Lond. B. Biol. Sci.* **160**:69.

FORTE, J. G., T. E. MACHEN, and T. M. FORTE. 1975. Ultrastructural and physiological changes in piglet oxyntic cells during histamine stimulation and metabolic inhibition. *Gastroenterology.* **69**:1208.

FRÖMTER, E. 1972. The route of passive ion movement through the epithelium of Necturus gallbladder. *J. Membr. Biol.* **8**:259.

HAMILTON, W. C. 1964. Statistics in Physical Science. Ronald Press, New York. 230.

LANCZOS, C. 1956. Applied Analysis. Prentice Hall, Inc., Englewood Cliffs, N.J. 272–280.

LEWIS, S. A. 1977. A reinvestigation of the function of the mammalian urinary bladder. *Am. J. Physiol.* **232(3)**:F187.

LEWIS, S. A., and J. M. DIAMOND. 1976. Na^+ transport by rabbit urinary bladder, a tight epithelium. *J. Membr. Biol.* **28**:1.

LEWIS, S. A., C. CLAUSEN, and J. M. DIAMOND. 1976*a*. Effective transepithelial capacitance. *J. Membr. Biol.* **28**:35.

LEWIS, S. A., D. C. EATON, and J. M. DIAMOND. 1976*b*. The mechanism of Na^+ transport by rabbit urinary bladder. *J. Membr. Biol.* **28**:41.

LEWIS, S. A., D. C. EATON, C. CLAUSEN, and J. M. DIAMOND. 1977. Nystatin as a probe for investigating the electrical properties of a tight epithelium. *J. Gen. Physiol.* **70**:427.

LINDEMANN, B. 1975. Impalement artifacts in microelectrode recordings of epithelial membrane potentials. *Biophys. J.* **15**:1161.

MACHEN, T. E., C. CLAUSEN, and J. M. DIAMOND. 1977. Electrical events during stimulation of HCl secretion by frog gastric mucosa *in vitro*. *Gastroenterology.* **73**:970.

MATHIAS, R. T., R. S. EISENBERG, and R. VALDIOSERA. 1977. Electrical properties of frog skeletal muscle fibers interpreted with a mesh model of the tubular system. *Biophys. J.* **17**:57.

NOYES, D. H., and W. S. REHM. 1970. Voltage response of frog gastric mucosa to direct current. *Am. J. Physiol.* **219**:184.

PESKOFF, A. 1979. Electrical potential in three-dimensional electrically syncytial tissues. *Bull. Math. Biol.* **41**:163.

PORTER, K. R., and M. A. BONNEVILLE. 1973. Fine Structure of Cells and Tissues. Lea & Febiger, Philadelphia, Pa. 108–109.

REHM, W. S., S. S. SANDERS, M. G. TANT, F. M. HOFFMAN, and J. T. TARVIN. 1976. Conductance of frog gastric mucosa under varying conditions as determined by square-wave analysis. *In* Gastric Hydrogen Ion Secretion. D. K. Kashekar, G. Sachs, and W. S. Rehm, editors. Marcel Dekker, Inc. New York. 29–53.

RICHTER, W. R., and S. M. MOIZE. 1963. Electron microscopic observations on the collapsed and distended mammalian urinary bladder (transitional epithelium). *J. Ultrastruct. Res.* **9**:1.

SMITH, P. G. 1975. Aldosterone-induced moulting in amphibian skin and its effect on electrical capacitance. *J. Membr. Biol.* **22**:165.

SMULDERS, A. P., J. McD. TORMEY, and E. M. WRIGHT. 1972. The effect of osmotically induced water flows on the permeability and ultrastructure of the rabbit gallbladder. *J. Membr. Biol.* **7**:164.

TEORELL, T. 1946. Application of "square wave analysis" to biological studies. *Acta Physiol. Scand.* **12**:235.

TEORELL, T., and R. WERSALL. 1945. Electrical impedance properties of surviving gastric mucosa of the frog. *Acta Physiol. Sand.* **10**:243.

VALDIOSERA, R., C. CLAUSEN, and R. S. EISENBERG. 1974*a*. Circuit models of the passive electrical properties of frog skeletal muscle fibers. *J. Gen. Physiol.* **63**:432.

VALDIOSERA, R., C. CLAUSEN, and R. S. EISENBERG. 1974*b*. Impedance of frog skeletal muscle fibers in various solutions. *J. Gen. Physiol.* **63**:460.

WALKER, B. E. 1960. Electron microscopic observations in transitional epithelium of the mouse urinary bladder. *J. Ultrastruct. Res.* **3**:345.